

A Reference Governor for Wheel-Slip Prevention in Railway Vehicles with Pneumatic Brakes

Danielson, Claus; Di Cairano, Stefano

TR2020-087 July 01, 2020

Abstract

This paper applies reference governor (RG) design to the problem of preventing excessive wheel-slip in railway vehicles with pneumatic brakes. The RG minimizes the difference between the desired and implemented deceleration set-point such that the system state remains inside a constraint admissible positive invariant set where wheel-slip is maintained below a prescribed level. This problem is complicated by the non-linear slip-dynamics and hysteresis in the pneumatic brake which results in a non-convex invariant set. The RG is evaluated in numerical simulations where we observe that the governor produces non-linear integral-action that has the beneficial properties of fast transient response and offset-free tracking while being robust to delays from hysteresis and uncertainty on the slip dynamics.

American Control Conference (ACC) 2020

A Reference Governor for Wheel-Slip Prevention in Railway Vehicles with Pneumatic Brakes

Claus Danielson[†] and Stefano Di Cairano[†]

Abstract—This paper applies reference governor (RG) design to the problem of preventing excessive wheel-slip in railway vehicles with pneumatic brakes. The RG minimizes the difference between the desired and implemented deceleration set-point such that the system state remains inside a constraint admissible positive invariant set where wheel-slip is maintained below a prescribed level. This problem is complicated by the non-linear slip-dynamics and hysteresis in the pneumatic brake which results in a non-convex invariant set. The RG is evaluated in numerical simulations where we observe that the governor produces non-linear integral-action that has the beneficial properties of fast transient response and offset-free tracking while being robust to delays from hysteresis and uncertainty on the slip dynamics.

I. INTRODUCTION

Regulating wheel-slip is a classic application of non-linear control theory. Traction control and anti-lock braking are two quintessential examples from automotive engineering in which the respective control objectives are to maximize the acceleration or deceleration according to the current environmental conditions [1], [2]. In other applications [3], [4], the control objective is to track a desired acceleration or deceleration set-point. For instance, automatic stopping of passenger trains requires precise tracking of the deceleration reference in order to stop the train at a specific location so that queued passengers can easily board the train.

Railway vehicles have different dynamics than automobiles and therefore have their own unique control challenges [5]. For instance, the friction between a steel wheel and rail is lower and has different characteristics than the friction between a rubber tire and asphalt [6]. Furthermore, the pneumatic brakes used on many trains have unique control design challenges due to their slow dynamics and non-linear hysteresis [7], [8]. To manage wheel-slip, many railway vehicles with pneumatic brakes employ a wheel-slip protection (WSP) system; when excessive wheel-slip is detected, the WSP vents gas from the brake cylinder to rapidly reduce braking torque, restoring the wheel-slip to the stable-slip region [9]. However, switching between the tracking controller and WSP can produce a limit cycle that causes excessive jerk, negatively effecting ride comfort for the passengers and increasing wear on the brake mechanism. Furthermore, overriding the brake tracking controller is undesirable for applications where precision stopping is desired since the slow dynamics and hysteresis mean that the brake requires a significant amount of time to recover after the WSP vents.

The main contribution of this paper is the application of reference governor (RG) theory for *preventing* excessive wheel-slip. The RG preemptively adjusts the deceleration reference to the brake controller to prevent excessive wheel-slip rather than reacting to incipient slip instability as is the case for the WSP system. Since the RG augments, rather than replaces, the existing controller, the extensive testing and carefully tuning of the existing controller is not wasted. Instead, the RG retains the performance of an existing linear controller, but adds the nonlinear feature of enforcing constraints on the wheel-slip. Another contribution of this paper is as a tutorial on

the application of theoretical non-convex RG design to the practical problem of stopping trains with pneumatic brakes.

The RG chooses the deceleration set-point closest to the desired reference from a state-dependent set of admissible references that are guaranteed to prevent excessive wheel-slip. Computing such an admissible set is challenging due to the non-linear slip dynamics and brake hysteresis. We model the nonlinearity and uncertainty of the slip dynamics using a polytopic differential inclusion and the brake hysteresis is modeled as a piecewise affine (PWA) system [10], [11]. This allows us to compute a non-convex constraint admissible positive invariant (PI) set which is represented by a union of convex polytopes.

This paper makes extensive use of RG [12] and invariant set theory [10], [13], [14]. In continuous-time, PI sets are called viable sets and the maximal PI is called the viability kernel [15]. Viability theory studies the existence of initial conditions for which constraint satisfaction is possible. However, it is non-constructive and therefore requires a controller to realize constraint enforcement e.g. a reference governor.

This paper is organized as follows. In Section II we describe the closed-loop dynamics of a railway vehicle pneumatic brake controller and formally define the wheel-slip *prevention* problem. In Section III we present our RG for wheel-slip prevention and discuss its efficient implementation. In Section IV we demonstrate the performance of our RG through numerical simulations.

Notation and Definition: A set $\mathcal{O} \subseteq \mathcal{X}$ is PI for the autonomous system $\dot{x} = f(x)$ if $f(x) \in \mathcal{O}$ for all $x \in \mathcal{O}$.

II. WHEEL-SLIP PROTECTION AND PREVENTION

Figure 1 shows a block-diagram of the components that comprises a pneumatic brake for a railway vehicle. In this section, we will describe each of these components and how their dynamics influence wheel-slip. We will then define the wheel-slip prevent problem.

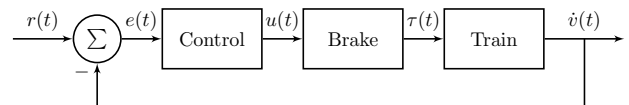


Fig. 1: Block diagram of a pneumatic brake for a railway vehicles, comprised of a controller, brake system, and the vehicle.

A. Railway Vehicle and Wheel-Slip Dynamics

In this section, we describe the models of the railway vehicle dynamics and wheel-slip dynamics.

The pneumatic brake produces a braking-torque $\tau(t)$ that reduces the angular speed $\omega(t)$ of the wheels, which in turn reduces the speed $v(t)$ of the vehicle. The dynamics of the speeds of the railway

[†] Mitsubishi Electric Research Laboratories (MERL), Cambridge MA

vehicle and wheel are modeled by

$$M\dot{v}(t) = -f(s) \quad (1a)$$

$$J\dot{\omega}(t) = rf(s) + \tau(t) \quad (1b)$$

where M is the mass of the vehicle, and J and r are the moment of inertia and radius of the wheel, respectively. The friction force $f(s) = \mu(s)N$ between the wheel and the rail can be modeled as the product of the normal force N and the friction coefficient $\mu(s)$, which is a nonlinear function (called the adhesion curve) of the wheel slip-speed $s(t)$. Here, slip-speed is defined as the difference between the vehicle speed $v(t)$ and the linear speed $r\omega(t)$ of the wheel

$$s(t) = v(t) - r\omega(t). \quad (2)$$

The slip-speed is defined to be positive $s(t) = v(t) - r\omega(t) \geq 0$ when the linear speed of the wheel is less than the speed of the vehicle $r\omega(t) \leq v(t)$, as occurs during braking. For railway-vehicles, wheel slip-speed is typically used rather than of slip-ratio $\frac{v(t) - r\omega(t)}{v(t)}$ which is commonly used in road-vehicle applications [5], [16].

The dynamics of the slip-speed $s(t)$ can be derived from the vehicle dynamics (1) and the definition of wheel slip-speed (2), yielding

$$\dot{s}(t) = -\left(\frac{1}{M} + \frac{r^2}{J}\right)f(s) + \frac{r}{J}\tau(t). \quad (3)$$

where $f(s) = \mu(s)N$ is the friction between the wheel and rail, and $\mu(s)$ is the adhesion-curve which describes how the friction coefficient depends on the slip-speed.

Many different adhesion-curves $\mu(s)$ have been suggested in the literature [5], [17], [18]. At low slip-speeds $s(t) \leq \bar{s}$, all these adhesion-curves are monotonic. Thus, the slip-dynamics (2) are (bound-input/bounded-output) stable i.e. the slip will increase $\dot{s}(t) > 0$ until the friction force $f(s) = \frac{Mr}{J+Mr^2}\tau$ balances the applied torque $\tau > 0$. In addition, the peak of the adhesion-curve $\mu(s)$ typically occurs in the low slip-speed region which means that maintaining low slip-speed yields faster stopping. Thus, it is desirable to keep the wheel-slip $s(t)$ in the low slip-speed region $s(t) \leq \bar{s}$, often called the stable-slip or adhesion region.

On the other hand, in the high slip-speed region $s(t) > \bar{s}$ the adhesion-curves may not be monotonic. Thus, if the braking torque $\tau > \frac{J+Mr^2}{Mr}\bar{f}$ is too large for the maximum friction force $\bar{f} = \bar{\mu}N$ to balance, then the slip-speed $s(t)$ will increase indefinitely $\dot{s}(t) > 0$. In practice, this means the wheel will be locked $\omega(t) = 0$ causing the slip-speed to reach its maximum value $s(t) = v(t)$, reducing the stopping force $f(s)$ applied to the vehicle (1). Thus, it is undesirable for the wheel-slip $s(t)$ to enter the high slip-speed region $s(t) > \bar{s}$, often called the unstable-slip region.

B. Pneumatic Brake Dynamics

In this section, we describe the pneumatic brake system and model its dynamics. Figure 2 shows a diagram of a pneumatic block-brake, but similar dynamics also apply to disk- and drum-brakes. Braking torque $\tau(t)$ is produced when the brake-block comes into contact with the wheel. The contact force is controlled by the pressure $p(t)$ in the brake-cylinder.

The brake-cylinder is filled from a reservoir, kept at a fixed pressure \bar{p} . The pressure $p(t)$ in the brake-cylinder is regulated by an integrated controller that modulates the valve opening to achieve a specified pressure. The specified pressure $u(t)$ is determined by the brake controller described in the next section. The response of

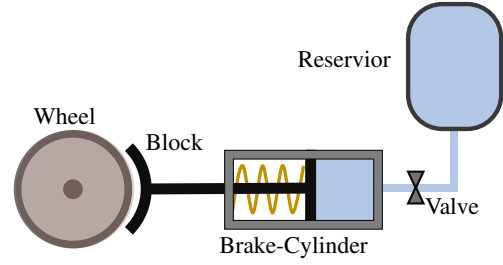


Fig. 2: Diagram of pneumatic brake system.

the actual brake-cylinder pressure $p(t)$ to the specified $u(t)$ pressure is modeled by a linear system

$$\dot{x}_p(t) = A_p x_p(t) + B_p u(t) \quad (4a)$$

$$p(t) = C_p x_p(t) + D_p u(t) \quad (4b)$$

where the dynamics (4) have unit dc-gain $C_p(I - A_p)^{-1}B_p + D_p = 1$ since the cylinder pressure $p(t)$ asymptotically tracks the reference pressure $u(t)$. We assume that the pressure $p(t)$ respond monotonically to the commanded pressure set-point $u(t)$.

The brake-cylinder pressure cannot be lower than ambient pressure $p = 0$ nor greater than the reservoir pressure. Similarly, the control input $u(t)$ cannot command a pressure outside the range of admissible pressures \bar{p} . Thus,

$$0 \leq p(t) \leq \bar{p} \quad (5a)$$

$$0 \leq u(t) \leq \bar{p}. \quad (5b)$$

Next, we consider the relationship between the brake-cylinder pressure and the braking-torque [7]. Nominally, increasing $\dot{p}(t) > 0$ the cylinder pressure $p(t)$ increases $\dot{\tau}(t) > 0$ the brake torque $\tau(t)$ while decreasing the pressure $\dot{p}(t) < 0$, decreases torque $\dot{\tau}(t) < 0$. However, when the brake-cylinder switches from filling $\dot{p}(t) > 0$ to venting $\dot{p}(t) < 0$, the brake torque initially does not respond $\dot{\tau}(t) = 0$. Likewise, $\dot{\tau}(t) = 0$ when switching from venting $\dot{p}(t) < 0$ to filling $\dot{p}(t) > 0$ as shown in Figure 3, which depicts the brake torque τ as a function of cylinder pressure p . The brake torque only increases $\dot{\tau}(t) > 0$ when the cylinder pressure $p(t)$ lies on the squeezing surface $\tau(t) = \bar{\alpha}p(t) + \bar{\beta}$. Likewise, the brake torque only decreases $\dot{\tau}(t) < 0$ along the releasing surface $\tau(t) = \underline{\alpha}p(t) + \underline{\beta}$. Otherwise, the brake torque is constant $\dot{\tau}(t) = 0$.

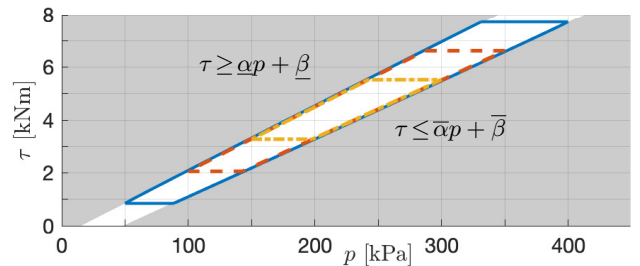


Fig. 3: Nonlinear relationship between brake-cylinder pressure $p(t)$ and the braking-torque $\tau(t)$

The nonlinear behavior of the brake shown in Figure 3 is modeled by the following hysteresis dynamics [7]

$$\dot{\tau}(t) = \begin{cases} \bar{\alpha}\dot{p}(t) & \text{if } \tau(t) = \bar{\alpha}p(t) + \bar{\beta}, \dot{p}(t) \geq 0 \\ \underline{\alpha}\dot{p}(t) & \text{if } \tau(t) = \underline{\alpha}p(t) + \underline{\beta}, \dot{p}(t) \leq 0 \\ 0 & \text{otherwise} \end{cases} \quad (6)$$

where the gains $\bar{\alpha}$ and $\underline{\alpha}$ describe how changes in the brake-cylinder pressure $\dot{p}(t)$ affect the change in braking torque $\dot{\tau}(t)$ when the braking-cylinder is being filled $\dot{p}(t) \geq 0$ and emptied $\dot{p}(t) \leq 0$, respectively. The torque remains constant $\dot{\tau}(t) = 0$ as the brake-cylinder pressure moves between the squeezing $\tau(t) = \bar{\alpha}p(t) + \bar{\beta}$ and releasing $\tau(t) = \underline{\alpha}p(t) + \underline{\beta}$ regions.

C. Brake Controller and Wheel-Slip Protection

The brake controller has two modes; reference tracking and slip protection. In the tracking mode, the control objective is to follow a deceleration command provided by an operator or higher-level controller. This is accomplished using a linear controller described by a linear system

$$\dot{x}_u(t) = A_u x_u(t) + B_u e(t) \quad (7a)$$

$$u(t) = C_u x_u(t) + D_u e(t) \quad (7b)$$

where the tracking error $e(t) = \dot{v}(t) - r(t)$ is the difference between the actual $\dot{v}(t)$ and desired $r(t)$ vehicle deceleration and the output of the controller (7) is the cylinder pressure set-point $u(t)$. The generic linear controller (7) is dynamic since it often includes integral-action for offset-free steady-state tracking e.g. a proportional-integral controller is typically used. Alternatively, if the controller is observer-based then (7) includes the observer dynamics.

If the slip-speed $s(t)$ enters the unstable-slip region $s(t) > \bar{s}$, then the controller enters the slip protection mode where the control objective is to return the slip-speed to the adhesion region. This is accomplished by venting the brake-cylinder pressure $p(t)$ which eventually reduces braking-torque $\tau(t)$ allowing the slip-speed $s(t)$ to reenter the adhesion region $s(t) \leq \bar{s}$. This is modeled by setting the desired brake-cylinder pressure to zero i.e. $u(t) = 0$.

D. Problem Statement: Wheel-Slip Prevention

The conflicting objectives of the WSP system and tracking controller can result in a limit cycle where the brake-cylinder pressure alternately is increased to produce the desired braking torque and vented to halt excessive slip. This limit cycle causes vibrations, reducing passenger comfort and increase wear on the brake mechanism. Thus, this paper proposes a wheel-slip prevention system which preemptively modifies the deceleration set-point to prevent the system from entering the unstable-slip region. The wheel-slip prevention problem is defined formally below.

Problem 1 (Wheel-Slip Prevention): Adjust the deceleration reference $r(t)$ such that the closed-loop brake system shown in Figure 1 satisfies the output constraints

$$\mathcal{Y} = \left\{ \begin{bmatrix} u \\ p \\ \tau \\ s \end{bmatrix} : \begin{array}{l} 0 \leq u, p \leq \bar{p} \\ s \leq \bar{s} \end{array} \right\}. \quad (8)$$

III. REFERENCE GOVERNOR FOR SLIP PREVENTION

In this section, we describe the design of a RG for solving Problem 1. Figure 4 shows a block diagram that illustrates how the RG interacts with the other elements of the closed-loop pneumatic brake system. The RG uses measurements or estimates of the controller state $x_u(t_k)$, pressure state $x_p(t_k)$, brake torque $\tau(t_k)$ and slip-speed $s(t_k)$ at time $t_k = k\Delta t$ to adjust the deceleration reference $r(t_k)$ to ensure that the constraints (8) are satisfied. In particular, the objective of the RG prevents the slip-speed $s(t_k)$ from leaving the stable-slip region $s(t_k) \leq \bar{s}$.

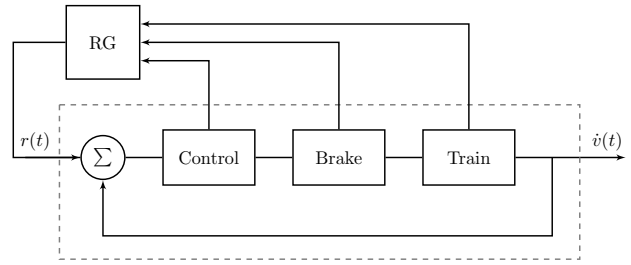


Fig. 4: Block diagram showing how the RG connects with the closed-loop brake system shown in Figure 1.

The RG takes the form of the a state-dependent non-convex optimization problem

$$r(t_k) = \arg \min_r |r - r^0(t_k)| \quad (9a)$$

$$\text{s.t. } r \in \mathcal{R}(x(t_k)) \quad (9b)$$

which minimizes (9a) the difference $|r - r^0(t_k)|$ between the requested $r^0(t_k)$ and implemented $r(t_k) = r^*$ deceleration set-points subject to the implemented reference r begin contained (9b) in a state-dependent set of admissible references $\mathcal{R}(x)$. The admissible set $\mathcal{R}(x)$ must be designed so that, not only are the constraints (8) satisfied at the current time $t_k = k\Delta t$, but also that it remains possible to satisfy them for all future times $t > k\Delta t$.

In the next section, Section III-A, we will describe how to model the nonlinear dynamics (3)-(4) and (6)-(7) of the brake system so that we can compute the state-dependent set of admissible references $\mathcal{R}(x)$ in Section III-B.

A. PWA Model of the Closed-Loop Brake System

In this section, we transform the nonlinear physics-based models from Section II into a hybrid model, specifically a discrete-time PWA system [10], [19]. PWA systems are a relatively simple class of hybrid systems, for which there are mature numerical tools [20] that can help us compute a PI set \mathcal{O} in the next section.

The cylinder pressure dynamics (4) and tracking controller dynamics (7) are already modeled as linear systems. Thus, we only need to convert (4) and (7) to discrete-time since linear systems are a special-case of PWA models. Furthermore, the constraints (5) on the cylinder pressure and control input are already polyhedral.

The brake-hysteresis (6) is modeled in discrete-time by

$$\tau = \begin{cases} \bar{\alpha}p + \bar{\beta} & \text{if } \tau^- \leq \bar{\alpha}p + \bar{\beta}, u \geq p \\ \underline{\alpha}p + \underline{\beta} & \text{if } \tau^- \geq \underline{\alpha}p + \underline{\beta}, u \leq p \\ \tau^- & \text{otherwise} \end{cases} \quad (10a)$$

where $p = p(t_k)$ and $\tau^- = \tau(t_{k-1})$ are the current cylinder-pressure and previous brake-torque, respectively, at the k -th sample-time $t_k = k\Delta t$. Note that (10a) only approximates the continuous-time hysteresis (6) since a mode (squeeze, release, hold) transition will almost surely occur between sample instances $[k\Delta t, (k+1)\Delta t]$ rather than at an exact sample instance $k\Delta t$. Thus, the torque $\tau(t_k)$ should be the sum of torques for each mode weighted by the fraction of time spend in that mode. However, since the sample-time rate is fast Δt relative to the system dynamics and torque varies continuously with pressure, the approximation (10a) is valid.

The constraint from (6) requiring that the brake-cylinder is not venting $\dot{p}(t) \geq 0$ in the squeeze region was replaced with the constraint $u(t_k) \geq p(t_k)$ in (10a). These constraints are

equivalent since we assumed that the pressure dynamics (4) respond monotonically to pressure commands $u(t)$. Using the constraint $u(t_k) \geq p(t_k)$ avoids the noise issues associated with numerically differentiating the pressure $\dot{p}(t) \approx \frac{p(t_k) - p(t_{k-1})}{\Delta t}$. In addition, we do not need an extra state p_{k-1} to keep track of the previously sampled pressure. Similarly, the constraint $\dot{p}(t) \leq 0$ from (6) requiring that the brake-cylinder is not filled in the release region was replaced with the equivalent constraint $u(t_k) \leq p(t_k)$.

Next, we address the nonlinearity and uncertainty in the slip dynamics (3) due to the nonlinear friction $f(s) = \mu(s)N$. It is unknown which, if any, of the nonlinear adhesion-curves $\mu(s)$ suggested in the literature [5], [17], [18] describes physical reality. Furthermore, the normal force N is uncertain due to aerodynamic effects, the inclination of the track, and variations in the mass due to the amount of cargo or number of passengers on the train.

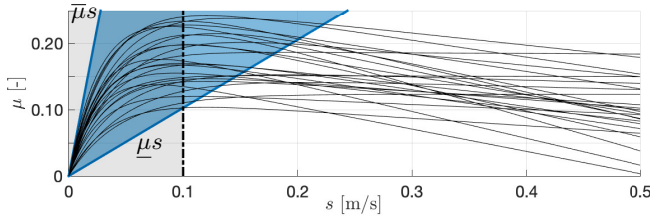


Fig. 5: Cone covering possible adhesion-curves $\mu(s)$ inside the stable-slip region $s \leq \bar{s}$

Our approach for dealing with this nonlinearity and uncertainty is motivated by Figure 5. Instead of considering an individual adhesion-curve, we consider a set that covers all the possible adhesion-curves $\mu(s)$ in the stable-slip region. The extreme linear adhesion-curves $\underline{\mu}s$ and $\bar{\mu}s$ bound the cone of possible adhesion-curves. Thus, the friction force $f(s) = \mu(s)N$ are bounded by the extreme linear friction-curves $\underline{f}s$ and $\bar{f}s$ where $\underline{f} = \underline{\mu}N$ and $\bar{f} = \bar{\mu}N$, and \underline{N} and \bar{N} are bounds on the normal force. The slip-dynamics (3) can then be bounded by the differential inclusion

$$\dot{s}(t) \in \left\{ -\frac{J+Mr^2}{MJ} f(s(t)) + \frac{r}{J} \tau(t) : \underline{f}s(t) \leq f(s(t)) \leq \bar{f}s(t) \right\}.$$

In discrete-time, the above differential inclusion can be modeled by the following scalar linear parametric differential inclusion

$$s(t_{k+1}) = a_s(\xi)s(t_k) + b_s(\xi)\tau(t_k) \quad (10b)$$

where $s(t_k)$ and $\tau(t_k)$ are the slip $s(t)$ and brake-torque $\tau(t)$ sampled at the k -th sample-time $t_k = k\Delta t$. The uncertain model parameters $a_s(\xi)$ and $b_s(\xi)$ are given by the convex combinations $a_s(\xi) = \xi \underline{a}_s + (1 - \xi) \bar{a}_s$ and $b_s(\xi) = \xi \underline{b}_s + (1 - \xi) \bar{b}_s$ where $(\underline{a}_s, \bar{a}_s)$ and $(\underline{b}_s, \bar{b}_s)$ are bounds on the parameters a_s and b_s respectively. The unknown time-varying parameter $\xi(t) \in [0, 1]$ accounts for both uncertainty and nonlinearity of the slip dynamics (3) due to the adhesion-curve. Since (10b) is a first-order system, only a single parameter $\xi \in [0, 1]$ is needed to cover the model uncertainty. Replacing the nonlinear slip-dynamics (3) with the uncertain linear dynamics (10b) does not adversely affect stability since the common Lyapunov function $V(s) = s^2$ is decreasing since $|a_s(\xi)| < 1$ for all $\xi \in [0, 1]$ when the slip-speed is low $s \leq \bar{s}$.

Piecewise Affine Dynamics: The discrete-time dynamics (10) can be combined into a single PWA system with polyhedral constraints

and parametric uncertainty

$$x(t_{k+1}) = \begin{cases} A_1 x(t_k) + B_1 r(t_k) + b_1 & \text{if } y(t_k) \in \mathcal{Y}_1 \\ A_2 x(t_k) + B_2 r(t_k) + b_2 & \text{if } y(t_k) \in \mathcal{Y}_2 \\ A_3 x(t_k) + B_3 r(t_k) + b_3 & \text{if } y(t_k) \in \mathcal{Y}_3 \end{cases} \quad (11a)$$

$$y(t_k) = Cx(t_k) + Dr(t_k) + d \quad (11b)$$

where the state $x(t_k) = [x_u(t_k), x_p(t_k), \tau(t_{k-1}), s(t_k)]^T$ is comprised of the current states of the controller $x_u(t_k)$ and cylinder pressure $x_p(t_k)$, the previous brake torque $\tau(t_{k-1})$, and the current wheel-slip $s(t_k)$. The constrained outputs $y(t_k) = [u(t_k), p(t_k), \tau(t_{k-1}), s(t_k)]^T$ are the current control input $u(t_k)$, current brake-cylinder pressure $p(t_k)$, the previous brake torque $\tau(t_{k-1})$, and the current wheel-slip $s(t_k)$. The three modes of the hybrid system (11) are the squeeze mode $i = 1$, release mode $i = 2$, and hold mode $i = 3$.

The regions $\mathcal{Y}_i \subseteq \mathbb{R}^4$ that determine where each mode (squeeze, release, hold) is active are subsets of the output-space \mathbb{R}^4 where the output of the closed-loop system (Figure 1) includes the brake controller input $u(t_k)$. The projections of these regions \mathcal{Y}_i onto the pressure-torque-input space $[p(t_k), \tau(t_{k-1}), u(t_k)]$ are shown in Figure 6. The slip $s(t_k)$ was left out of Figure 6 since the regions \mathcal{Y}_i only have simple bounds on the slip $s(t_k)$ and do not have any constraints that couple slip with the other states or the input. In other words, the sets \mathcal{Y}_i are prismatic in the slip $s(t_k)$ direction.

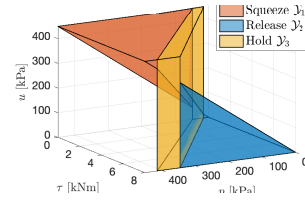


Fig. 6: Squeeze \mathcal{Y}_1 , release \mathcal{Y}_2 , and hold \mathcal{Y}_3 regions for the hybrid dynamics (11).

The pressure-torque relationship for the squeeze region $\mathcal{Y}_1 \subseteq \mathcal{Y}$ is the same as shown in Figure 3. The squeeze region \mathcal{Y}_1 has an additional constraint $p(t_k) \leq u(t_k)$ requiring that the pressure $p(t_k)$ is not being vented. Likewise, the release region \mathcal{Y}_2 has a constraint that the brake-cylinder $p(t_k) \geq u(t_k)$ is not being filled. In (6) the hold region was defined as states not in the squeeze \mathcal{Y}_1 or release \mathcal{Y}_2 regions. From 6 it is clear that the resulting region $\mathcal{Y} \setminus (\mathcal{Y}_1 \cup \mathcal{Y}_2)$ would be non-convex. However, since in practice the state will only belong to the boundaries of the squeeze \mathcal{Y}_1 and release \mathcal{Y}_2 regions, the hold region \mathcal{Y}_3 was defined as the entire region between the squeeze and release surfaces i.e. $\mathcal{Y}_3 = \{x : \bar{\alpha}p + \bar{\beta} \leq \tau \leq \underline{\alpha}p + \underline{\beta}\}$.

B. Set of Admissible References

In this section, we show how to compute the set of admissible references $\mathcal{R}(x)$ used by the RG (9) to ensure that the constraints (8) are satisfied.

Following the design [12] of RGs, we first augment the closed-loop dynamics (11) with a constant $r(t_{k+1}) = r(t_k)$ reference

$$\hat{x}^+ = \hat{f}_\xi(\hat{x}) = \begin{cases} \hat{A}_1 \hat{x} + \hat{b}_1 & \text{if } \hat{x} \in \hat{\mathcal{X}}_1 \\ \hat{A}_2 \hat{x} + \hat{b}_2 & \text{if } \hat{x} \in \hat{\mathcal{X}}_2 \\ \hat{A}_3 \hat{x} + \hat{b}_3 & \text{if } \hat{x} \in \hat{\mathcal{X}}_3 \end{cases} \quad (12)$$

where the augmented state $\hat{x}(t_k) = [x(t_k), r(t_k)]^T \in \mathbb{R}^{n_x+1}$ includes the closed-loop system (11) state $x(t_k) \in \mathbb{R}^{n_x}$ and the reference $r(t_k) \in \mathbb{R}^1$. The parameters are $\hat{A}_i(\xi) = \begin{bmatrix} A_i(\xi) & B_i \\ 0 & I \end{bmatrix}$, $\hat{b}_i =$

$\begin{bmatrix} b_i \\ 0 \end{bmatrix}$, and $\mathcal{X}_i = \{ \begin{bmatrix} x \\ r \end{bmatrix} : \begin{bmatrix} C & D \end{bmatrix} \begin{bmatrix} x \\ r \end{bmatrix} + d \in \mathcal{Y}_i \}$ for $i=1, 2, 3$. We then compute a constraint admissible PI set using the approach from [10] of iteratively backward propagating the system constraints (8) through the system dynamics (12)

$$\Omega^0 = \hat{\mathcal{X}} \quad (13a)$$

$$\Omega^{k+1} = \bigcap_{\xi \in \{0,1\}} \hat{f}_\xi^{-1}(\Omega^k) \cap \hat{\mathcal{X}} \quad (13b)$$

where \hat{f}_ξ^{-1} is the pre-image of the augmented dynamics (12) for $\xi=0,1$ and $\hat{\mathcal{X}} = \{ \hat{x} : Cx + Dr + d \in \mathcal{Y} \}$ is the set of augmented states \hat{x} corresponding to outputs y that satisfy the constraints (8). The maximal constraint admissible PI set $\mathcal{O} = \lim_{k \rightarrow \infty} \Omega^k$ is the limit of the iteration (13).

The state-dependent set of admissible references $\mathcal{R}(x)$ is the set of constant references $r(t_{k+1}) = r(t_k)$ such that the closed-loop system (11) satisfies constraints (8) for all future times i.e.

$$\mathcal{R}(x) = \{ r : \begin{bmatrix} x \\ r \end{bmatrix} \in \mathcal{O} \}. \quad (14)$$

The iteration (13) is complicated by the fact that the augmented brake dynamics (12) are nonlinear. Fortunately, the PWA dynamics and polyhedral constraints of the hybrid model (12) mean that the non-convex backward-reachable sets Ω_k can be expressed as a union of convex polyhedrons [21]

$$\Omega^k = \bigcup_j \Omega_j^k \quad (15)$$

where $\Omega_j^k = \{ \hat{x} : H^j \hat{x} \leq h^j \}$ is the j -th convex polyhedron defining the union Ω^k . The backward propagation (13) can thus be implemented by computing the pre-image of each component Ω_j^k of the set Ω_k under each mode $i=1, 2, 3$ of the dynamics (12). The new component sets Ω_{k+1}^j of Ω_{k+1} are polytopes given by $\Omega_{k+1}^{j'} = (\hat{A}_i^{-1} \Omega_j^k - \hat{A}_i^{-1} b_i) \cap \mathcal{X}_i$ for $j=1, \dots, J$ and $i=1, 2, 3$ where $\Omega_j^k = \{ \hat{x} : H^j \hat{x} \leq h^j \}$ and $\mathcal{X}_i = \{ \hat{x} : G_i \hat{x} \leq g_i \}$.

IV. EVALUATION OF THE REFERENCE GOVERNOR

In this section, we test our RG for wheel-slip prevention through numerical simulation. For this test case, the pressure dynamics (4) are modeled by a simple first-order system $\dot{p}(t) = -\frac{1}{T_p}(p(t) - u(t))$ with a $T_p = 50$ millisecond delay. The controller (7) is a simple proportional-integral controller

$$u(t) = K_P e(t) + K_I \int_0^t e(\sigma) d\sigma \quad (16)$$

where K_P and K_I are the proportional and integral gains respectively, and the tracking error $e(t) = r(t) - \dot{v}(t)$ is the difference between the desired $r(t)$ and actual $\dot{v}(t)$ deceleration of the vehicle. The actual deceleration $\dot{v}(t)$ is directly measured using an accelerometer.

Figure 7 shows the maximal PI set $\mathcal{O} \subset \mathbb{R}^5$ for the closed-loop brake system. Figure 7a shows the PI set \mathcal{O} sliced along in the squeeze plane $\tau = \bar{\alpha}p + \bar{\beta}$ and equilibrium brake pressure plane $u = p$. Likewise, Figure 7b shows a slice of the PI set \mathcal{O} in the subspace $\tau = \underline{\alpha}p + \underline{\beta}$ and $u = p$. The wheel-slip prevention RG (9) uses the PI set \mathcal{O} to determine the set of admissible constant deceleration set-points (14). The RG (9) adjusts the deceleration set-point $r(t)$ to ensure that the closed-loop system satisfies constraints (8). In particular, the RG ensures that the slip-speed $s(t)$ remains inside the adhesion-region $s(t) \leq \bar{s} = 0.1$. Thus, the reference $r(t)$ is severely limited in the squeeze mode (Figure 7a) when the slip $s \gg 0$ and torque $\tau \gg 0$ are high. The reference $r(t)$ is less restricted in the release mode (Figure 7b) since the brake can quickly reduce torque τ to prevent excessive slip $s > 0.1$.

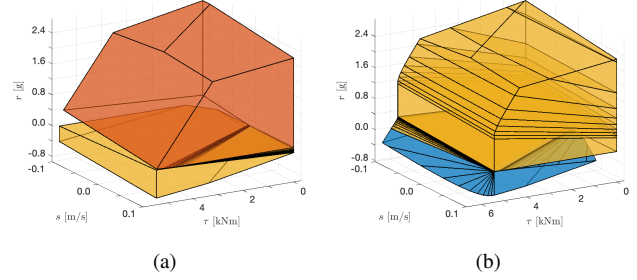


Fig. 7: PI set \mathcal{O} for (12) with $r(t_{k+1}) = r(t_k)$. (a) Slice of \mathcal{O} along squeeze plane. (b) Slice of \mathcal{O} along release plane.

A. Prevention of Wheel-Slip

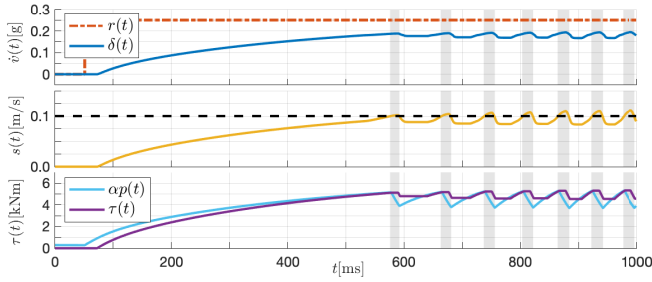
In this section, we show that the wheel-slip prevention RG prevents the controller from entering the WSP mode, described in Section II-C.

We consider a scenario in which the peak wheel-rail friction $f_{max} = 0.2Mg$ is too low to achieve the desired deceleration set-point $r^0(t) = 0.25g$. Without the RG, the wheel-slip $s(t)$ exceeds the stable-slip threshold $s(t) > 0.1$ causing the brake controller to enter the WSP mode which produces the undesirable oscillatory behavior shown in Figure 8a. In WSP mode, the brake-cylinder pressure $p(t)$ is quickly vented to reduce braking torque $\tau(t)$ and restore the slip $s(t)$ to the stable-slip region $s(t) \leq 0.1$. Unfortunately, this severely disrupts the tracking controller causing the deceleration tracking error $r^0(t) - \dot{v}(t)$ to increase. Even after the WSP mode is disengaged and the tracking controller is re-engaged, the undesirable behavior persists; the tracking controller requires approximately 100 milliseconds to overcome the brake hysteresis and then another approximately 400 milliseconds to achieve the previous deceleration peak, at which point the wheel-slip $s(t)$ again exceeds the threshold $s(t) > 0.1$ and the WSP mode is again engaged. The resulting limit cycle has a relatively large average deceleration tracking error $\lim_{T \rightarrow \infty} \frac{1}{T} \int_0^T r^0(t) - \dot{v}(t) dt \approx 0.0718g$.

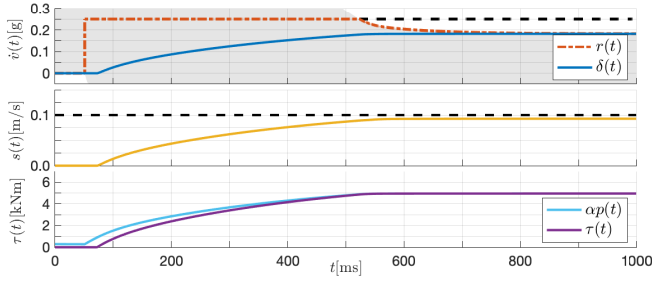
Figure 8b shows that the RG prevents the slip-speed from entering the unstable-slip region, eliminating the previous undesirable behavior shown Figure 8a. As the slip $s(t)$ approaches the boundary of the stable-slip region, the RG lowers the infeasible desired reference $r^0(t) = 0.25g$ to an achievable reference $r(t) \approx 0.2g$. This results in a non-zero steady-state tracking error $\lim_{t \rightarrow \infty} r^0(t) - \dot{v}(t) \approx 0.0682g$ which is lower than the average tracking error that results from not using the RG. It is important to note that a small improvement in deceleration tracking can lead to a large improvement in stopping accuracy since position error is proportional to the double-integral of deceleration error. Over a 30 seconds braking maneuver, the RG improves the stopping accuracy by 1.62 meters, which is very large compared with the desire stopping accuracy of $O(10)$ centimeters [4]. Most importantly, the smoother deceleration profile (Figure 8b) produced by the RG causes less jerk than the WSP (Figure 8a), resulting in a more comfortable ride for the passengers and reduced wear on the braking mechanism.

B. Aggressive Controller

The aggressiveness of the proportional-integral controller (16) is fundamentally limited by the brake hysteresis and adhesion-curve nonlinearity. Aggressive integral-action can cause overshoot and windup. Both of these issues are aggravated by plant nonlinearity.



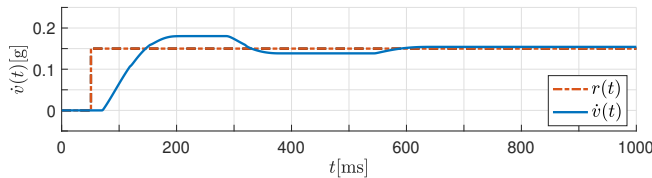
(a) Simulations of the brake-system *without* the RG which produces undesirable cycling due to WSP. The shaded regions show times when the WSP system was engaged.



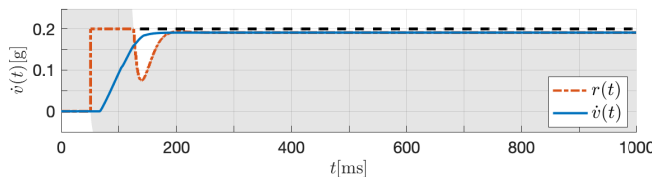
(b) Simulations of the brake-system *with* the RG showing the elimination of cycling. The shaded regions show state-dependent bounds on the reference calculated by RG.

Fig. 8: Simulation with an infeasible deceleration set-point.

Overshoot can cause the slip-speed to enter the unstable-slip region even when the steady-state deceleration set-point is feasible. The delay caused by the hysteresis shown in Figure 3 can cause the integrator to windup which can lead to oscillatory behavior or even instability. In terms of classical control, the hysteresis delay means that the closed-loop system (Figure 1) must have a large phase margin which limits the aggressiveness of the tracking controller. In this section, we show that the wheel-slip prevention RG mitigates both of these issues allowing the use of a more aggressive controller.



(a) Simulations of the brake-system *without* the RG which results in overshooting and cycling caused by aggressive integral-action.



(b) Simulations of the brake-system *with* the RG showing inherent anti-windup

Fig. 9: Simulation with an aggressive controller.

Figure 9a shows the closed-loop response of the braking system to a feasible deceleration command. The more aggressive controller settles approximately three times faster than the previous controller

shown in Figure 8. In fact, the oscillations produced by the integral-action prevent even faster convergence since each oscillation needs to pass through the hold zone in Figure 3. In addition, the closed-loop response in Figure 9a has a small overshoot which can be a problem near the boundary of the stable-slip region. Figure 9b shows that the RG mitigates both the issues.

Figure 9b shows the closed-loop response of the braking system to a deceleration command on the boundary of the stable-slip region. As the deceleration $\dot{v}(t)$ approaches the set-point $r^0(t)$, the RG decreases the reference $r(t)$. This unwinds the integrator in the controller producing two beneficial effects. First, the slip-speed remains in the stable region. Second, the oscillations are greatly attenuated allowing the vehicle deceleration to converge more quickly to the desired set-point. Essentially, the RG produces non-linear integral-action that has the beneficial properties of fast transient response and offset-free tracking without the disadvantage of poor robustness to model uncertainty and delays, normally associated with aggressive integral-action.

REFERENCES

- [1] U. Kiencke and L. Nielsen, *Automotive Control Systems: For Engine, Driveline and Vehicle*. Springer-Verlag, 2000.
- [2] V. Ivanov, D. Savitski, and B. Shyrokau, "A survey of traction control and antilock braking systems of full electric vehicles with individually controlled electric motors," *Trans on Vehicular Technology*, 2014.
- [3] Y. Cheng, S. Haghghat, and S. Di Cairano, "Robust dual control mpc with application to soft-landing control," *American Control Conference*, 2015.
- [4] C. Danielson and S. Di Cairano, "Robust soft-landing control with quantized input," *Symposium on Nonlinear Control Systems*, 2016.
- [5] S. Park, J. Kim, J. Choi, and H. Yamazaki, "Modeling and control of adhesion force in railway rolling stocks," *Control Systems Magazine*, 2008.
- [6] O. Polach, "Creep force in simulations of traction vehicles running on adhesion limit," *Wear*, 2005.
- [7] D. Lee and C. Kang, "A mechanical brake hardware-in-the-loop simulation of a railway vehicles that accounts for hysteresis and pneumatic cylinder dynamics," *Advances in Mechanical Engineering*, 2015.
- [8] J. Oh, B. Drincic, and D. Bernstein, "Nonlinear feedback models of hysteresis," *Control Systems Magazine*, 2009.
- [9] S. Iwnicki, *Handbook of Railway Vehicle Dynamics*. CRC Press, 2006.
- [10] S. Raković, P. Grieder, M. Kvasnica, D. Mayne, and M. Morari, "Computation of invariant sets for piecewise affine discrete time systems subject to bounded disturbances," in *Conference on Decision and Control*, 2004.
- [11] R. Goebel, R. Sanfelice, and A. Teel., *Hybrid dynamical systems*. Princeton University Press, 2012.
- [12] I. V. Kolmanovskiy, E. Garone, and S. D. Cairano, "Reference and command governors: A tutorial on their theory and automotive applications," *2014 American Control Conference*, 2014.
- [13] F. Blanchini and S. Miani, *Set-Theoretic Methods in Control*. Birkhäuser, 2007.
- [14] F. Borrelli, A. Bemporad, and M. Morari, *Predictive Control for Linear and Hybrid Systems*, 2012.
- [15] J.-P. Aubin, *Viability Theory*. Birkhauser Boston Inc., 1991.
- [16] D. Frylmark, S. Johnsson, F. Botling, and M. Eriksson, "Automatic slip control for railway vehicles," Master's thesis, Linkopings, 2003.
- [17] C. de Wit, H. Olsson, K. Astrom, and P. Lischinsky, "A new model for control of systems with friction," *Trans on Automatic Control*, 1995.
- [18] V. van Geffen, "A study of friction models and friction compensation," Master's thesis, Eindhoven, 2009.
- [19] P. Biswas, P. Grieder, J. Löfberg, and M. Morari, "A survey on stability analysis of discrete-time piecewise affine systems," in *IFAC World Congress*, 2005.
- [20] M. Herceg, M. Kvasnica, C. Jones, and M. Morari, "Multi-Parametric Toolbox 3.0," in *European Control Conference*, 2013.
- [21] A. Bemporad, K. Fukuda, and F. D. Torrisi, "Convexity recognition of the union of polyhedra," *Computational Geometry*, 2000.